

Effects of tool geometry and process parameters on delamination in CFRP drilling: An overview

*Original*

Effects of tool geometry and process parameters on delamination in CFRP drilling: An overview / Melentiev, R., Priarone, P.C., Robiglio, M., Settineri, L.. - 45:(2016), pp. 31-34. (3rd CIRP Conference on Surface Integrity (CIRP CSI) Charlotte (NC), USA 8-10 Giugno 2016) [10.1016/j.procir.2016.02.255].

*Availability:*

This version is available at: 11583/2647562 since: 2016-09-07T12:51:47Z

*Publisher:*

Elsevier B.V.

*Published*

DOI:10.1016/j.procir.2016.02.255

*Terms of use:*

This article is made available under terms and conditions as specified in the corresponding bibliographic description in the repository

*Publisher copyright*

(Article begins on next page)



# Cost competitiveness of green ammonia via solid oxide electrolysis in Europe: A region-specific analysis

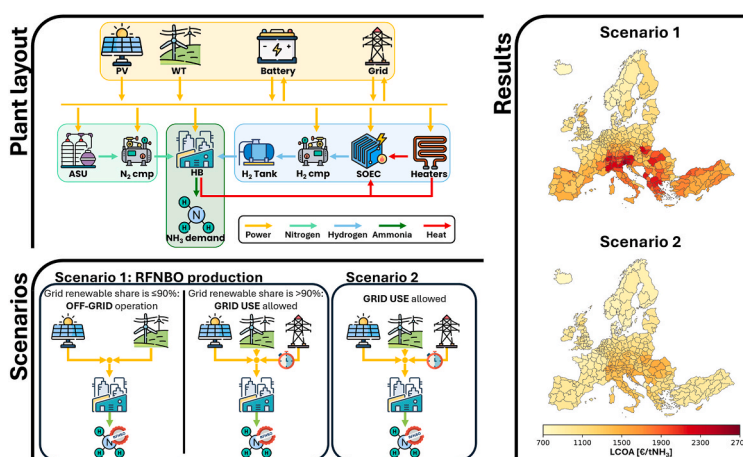
Alessandro Magnino <sup>\*</sup>, Paolo Marocco, Massimo Santarelli, Marta Gandiglio

Department of Energy, Politecnico di Torino, Corso Duca degli Abruzzi 24, Torino, 10129, Torino, Italy

## HIGHLIGHTS

- Impact of RFNBO requirements on electrolytic ammonia production in Europe.
- Detailed modelling of SOEC efficiency curve for more accurate plant modelling.
- Heat integration with Haber-Bosch enhances SOEC system performance.
- Windy regions emerge as the most cost-effective for ammonia production.
- Grid electricity lowers costs and storage needs, especially in sunny regions.

## GRAPHICAL ABSTRACT



## ARTICLE INFO

### Keywords:

Solid oxide electrolysis cell  
 Levelised cost of ammonia  
 Decarbonisation  
 Mixed integer linear programming

## ABSTRACT

Ammonia is a vital commodity for both agriculture and industry, with global demand projected to exceed 680 million tonnes annually by 2050. However, conventional ammonia production via the Haber-Bosch process, which relies on fossil-derived hydrogen, is highly carbon intensive. Decarbonising ammonia production is therefore essential to achieve net-zero targets and reduce fossil fuel dependency. This study develops a comprehensive Mixed Integer Linear Programming model to optimise green ammonia production across Europe based on high-efficiency solid oxide electrolysis. The model incorporates a detailed efficiency curve of the electrolyser together with its specific thermal requirements, effectively capturing operational synergies between the electrolysis system and the Haber-Bosch reactor through integrated heat management. The analysis evaluates the optimal Levelised Cost Of Ammonia (LCOA) under different configurations – islanded and grid-connected – highlighting the implications of the revised EU Renewable Energy Directive (RED III) on renewable energy use, system design and costs. The results identify regions with high wind potential (e.g., northern France, Denmark, England) as the most cost-competitive for ammonia production, achieving LCOA values of around 1000 €/tNH<sub>3</sub>. These regions benefit from higher average capacity factors and better temporal alignment between renewable generation and plant electricity demand compared to solar-dominated regions. In contrast, areas with limited

<sup>\*</sup> Corresponding author.

E-mail address: [alessandro.magnino@polito.it](mailto:alessandro.magnino@polito.it) (A. Magnino).

wind resources and high solar availability, such as southern Europe, are less competitive, with LCOA values exceeding 1800 €/tNH<sub>3</sub>, mainly due to the day-night shift in energy production. Grid electricity integration is shown to reduce costs by enabling the downsizing of both storage systems and renewable generation capacity; however, it also introduces additional variability related to local grid electricity prices and carbon intensity. Overall, this work provides actionable insights for the development of cost-effective, region-specific green ammonia plants, supporting the transition towards sustainable ammonia production in line with European energy and climate goals.

## 1. Introduction

Ammonia (NH<sub>3</sub>) is a fundamental commodity and a precursor to nitrogen-based products, particularly fertilisers (IEA, 2021; IRENA, AEA, 2022), whose use is expected to increase with global population (Gabrielli et al., 2023). Additionally, NH<sub>3</sub> is utilised in various other applications, such as refrigeration, mining, pharmaceuticals, water treatment, and plastics (IRENA, AEA, 2022; Zumdahl, 2024), with increasing attention to its uses as a fuel and energy carrier (Herbinet et al., 2022; Liu and Fu, 2025; Wang et al., 2025). Consequently, the International Renewable Energy Agency (IRENA) estimates that global NH<sub>3</sub> demand, currently around 180 million tonnes per year (International Fertilizer Industry Association, 2024), could exceed 680 million tonnes per year by 2050 (IRENA, AEA, 2022).

Industrial-scale NH<sub>3</sub> production is predominantly carried out via the Haber-Bosch (HB) process, which synthesises NH<sub>3</sub> from hydrogen (H<sub>2</sub>) and nitrogen (N<sub>2</sub>) feedstocks. Today, H<sub>2</sub> is mainly produced from fossil fuels (coal and natural gas (IEA, 2021)), making NH<sub>3</sub> synthesis a major carbon dioxide (CO<sub>2</sub>) emitter: about 500 Mt annually, corresponding to roughly 1% of global emissions and 15–20% of the chemical sector (IRENA, AEA, 2022). In Europe, about 36 MtCO<sub>2</sub>/y originate from NH<sub>3</sub> plants, as over 85% of hydrogen still comes from Steam Methane Reforming (SMR) (Mingolla et al., 2024). Therefore, the decarbonisation of NH<sub>3</sub> production is essential for achieving carbon neutrality by 2050 (European Commission, 2020) and ending the dependence of the European Union (EU) on Russian natural gas (European Commission, 2022).

Researchers are exploring the possibility of replacing the HB process with more sustainable direct electrochemical reduction of N<sub>2</sub> (Soloveichik, 2019; Suryanto et al., 2021; Wu et al., 2021). This alternative method promises greater flexibility in terms of operational scale and a lower carbon footprint. However, the electrochemical reduction process remains far from being a viable replacement for the HB process at an industrial scale. At present, the most promising strategy for rapidly decarbonising NH<sub>3</sub> production involves coupling the well-established HB process with sustainable hydrogen production methods based on water electrolysis. Electrolysers enable H<sub>2</sub> production by exploiting Renewable Energy Sources (RES), allowing integration upstream of the HB reactor for NH<sub>3</sub> synthesis. This approach has the potential to eliminate direct CO<sub>2</sub> emissions associated with the NH<sub>3</sub> synthesis process, provided that the electricity supply for hydrogen production is fully renewable. In fact, it should be noted that the carbon intensity of grid electricity in most EU countries does not guarantee lower emissions in hydrogen production compared to conventional SMR when electrolysers are powered by grid electricity (Magnino et al., 2025; Mayer et al., 2023).

Achieving both technical feasibility and cost-effectiveness in green ammonia production requires optimal system design, focused on minimising Levelised Cost Of Ammonia (LCOA). Various studies have investigated this challenge under different assumptions and configurations. One of the main differences lies in the operational setup: whether the plant is grid-connected, islanded or semi-islanded. In grid-connected configurations, several studies exploit grid electricity to reduce or eliminate on-site generation and storage requirements, thereby decreasing capital costs. Fúnez Guerra et al. (2020) performed a techno-economic assessment for a green ammonia supply chain

(Chile–Japan), showing how grid interaction affects optimal system sizing and cost structure, while Gomez et al. (2020) combined techno-economic and life-cycle assessment approaches to highlight that grid dependence can shift both costs and emissions. Zhang et al. (2020) compared alternative green ammonia process routes and discussed how system-level heat recovery options (e.g., steam cycles) can reduce energy demand under grid-connected operation. However, as highlighted by Mayer et al. (2023) and Magnino et al. (2025), reliance on grid electricity to power electrolysers may lead to CO<sub>2</sub> emissions comparable to or higher than those from SMR under the current EU electricity mix. Moreover, such systems may be exposed to electricity price fluctuations, potentially leading to increased production costs. To mitigate these drawbacks, multiple works focus on off-grid plants powered by photovoltaic (PV) and/or wind, where storage becomes a key design driver. Nayak-Luke et al. (2018) explicitly linked renewable intermittency to the required oversizing and storage needs of islanded ammonia plants, while Wang et al. (2023) investigated how Haber-Bosch operational flexibility impacts the optimal renewable configuration and storage sizing. Finally, Florez et al. (2024) extended the off-grid optimisation framework to export-oriented systems, highlighting the trade-off between islanded design, storage, and delivered product costs.

Recently, semi-islanded plants have emerged as a promising compromise. Studies by Salmon and Bañares-Alcántara (2021) and Campion et al. (2023) showed that semi-islanded setups can significantly reduce the need for large energy storage systems, resulting in more cost-effective solutions. On the other hand, emissions can still be high, resulting in embedded CO<sub>2</sub> emissions comparable to those of fossil fuels-based systems (Campion et al., 2023).

Another critical factor influencing plant performance and cost is the choice of the electrolyser technology, which affects both capital investment and energy consumption. Most studies have focused on mature low-temperature electrolysers. Armijo and Philibert (2020) investigated flexible green ammonia production under variable wind and solar availability, while Morgan et al. (2017) reviewed offshore wind potential for ammonia production and, more recently, Yu et al. (2024) proposed an optimisation-based sizing and operation model for isolated RES system couples to an ammonia synthesis loop, all highlighting the attractiveness of Alkaline Electrolysis Cells (AECs). Proton Exchange Membrane Electrolysis Cells (PEMECs)-based configurations have also been widely assessed in plant-level case studies, such as the Chile-Japan supply chain in Fúnez Guerra et al. (2020) and the North European energy system by Ikaheimo et al. (2018) and the Iranian case studies presented by Kakavand et al. (2023), all exploiting the operational flexibility given by this technology.

By contrast, only a few have explored the potential of Solid Oxide Electrolysis Cells (SOECs) (Campion et al., 2023; Nami et al., 2022; Schiedeck et al., 2025). Despite higher capital costs, SOEC technology offers greater efficiency (Luo et al., 2014; Nejjadian et al., 2022) compared to alternative methods, often making it the most cost-effective solution (Magnino et al., 2025). Moreover, coupling a SOEC with the Haber-Bosch reactor is particularly effective, as waste heat from NH<sub>3</sub> synthesis can be exploited by the SOEC auxiliary system for water pre-heating. Cinti et al. (2017) were among the first to analyse the benefits of integrating SOECs and the HB process on overall efficiency. More recently, Nowicki et al. (2023) proposed an integrated SOEC-HB loop combined with solid electrolyte oxygen pumps, further

emphasising the system-level opportunities enabled by high-temperature integration. [Schiedeck et al. \(2025\)](#) highlighted additional benefits under flexible operation by investigating the possibility of reducing the operational load of the HB process. In parallel, the literature also examines solid oxide fuel cell-based concepts, typically in power-to-ammonia-to-power systems exploiting reversible cells ([Mukelabai et al., 2021](#)). While relevant to the broader electrolysis–ammonia energy system perspective, these studies focus on mode switching and power generation rather than on continent-scale optimisation of SOEC-HB ammonia production.

Since the electrolyser accounts for the largest share of the plant's electrical demand ([Cinti et al., 2017](#)), accurately modelling its performance is essential. While most studies assume a constant efficiency for the electrolyser ([Armijo and Philibert, 2020](#); [Campion et al., 2023](#); [Cinti et al., 2017](#)), considering a part-load performance curve is crucial for assessing energy consumption under flexible operation.

Finally, site selection is also a key factor in determining the cost of electrolytic-based ammonia. For RES-based electricity, the renewable energy potential at a given location directly affects the sizing of system components and, consequently, investment costs, as demonstrated at the global level by [Fasihi et al. \(2021\)](#) and for the United States by [Bose et al. \(2022\)](#). In grid-connected configurations, location is equally important, as regional electricity prices and carbon intensity vary significantly. In both cases, the cost of electricity, one of the most influential factors in ammonia production economics, is heavily shaped by geographical location ([Sousa et al., 2022](#)).

### 1.1. Aims and novelty

This study addresses the previously outlined limitations in existing research by developing an optimisation model for green ammonia synthesis based on SOEC technology. It builds on previous work by the authors, which demonstrated the competitiveness of solid oxide electrolysis against other electrolyser technologies and SMR due to its high efficiency and effective heat integration in NH<sub>3</sub> production ([Magnino et al., 2025](#)).

A Mixed Integer Linear Programming (MILP) framework is formulated to explore both optimal component sizing and operational strategies aimed at minimising LCOA. Unlike most existing literature, the electrolyser model includes a detailed efficiency curve derived from process-level analysis, enabling an accurate representation of SOEC performance over the full modulation range. The model also accounts for thermal management challenges specific to high-temperature electrolysis by incorporating warm stand-by energy requirements during idle periods, generally overlooked in previous studies, and captures heat integration between the SOEC and HB reactor to improve overall system efficiency.

The optimisation framework is applied within a European context, enabling a region-specific (NUTS 2) evaluation of NH<sub>3</sub> production costs based on local renewable energy potential, under both islanded and grid-connected scenarios. Given the current regulatory landscape in Europe, these scenarios are designed to assess the implications of the 2023 update of the EU Renewable Energy Directive (RED III) ([European Commission, 2023a](#); [European Parliament, 2023](#)) on the cost-competitiveness of green ammonia, accounting for regulatory variations across regions. Region-specific grid electricity prices and carbon intensities are used to provide a realistic evaluation of grid dependency, assessing both costs and ammonia carbon intensity in case grid electricity use is allowed.

Beyond estimating regional LCOA, the study identifies optimal plant configurations adapted to local resource availability, highlighting how RES potential shapes both system design and production cost.

The remainder of this paper is structured as follows: Section 2 outlines the methodology, including a detailed description of the plant components, optimisation strategy, and modelling constraints. Results and discussion are presented in Section 3, while conclusions are drawn

in Section 4.

## 2. Methods

This section presents a description of the scenarios, optimisation methodology, and the main plant components. Section 2.1 introduces the analysed scenarios and their respective constraints, Section 2.2 details the optimisation methodology employed in the study (an illustrative scheme is reported in [Fig. 1](#)), Section 2.3 provides an overview of the plant configuration, while regional data regarding RES potential are shown in Section 2.4. Sections 2.5 to 2.8 describe the main characteristics of the plant subsystems, specifically those related to electricity, hydrogen, nitrogen and ammonia.

### 2.1. Scenarios

In response to the urgent need to accelerate the EU clean energy transition, the revision of Directive (EU) 2018/2001, commonly referred to as RED III ([European Parliament, 2023](#)), entered into force in November 2023. This directive maintains the specific requirements for producing hydrogen-derived products, such as ammonia, as detailed by the Commission Delegated Regulation (EU) 2023/1184 ([European Commission, 2023b](#)), supplementing RED II. To qualify as Renewable Fuel of Non-Biological Origin (RFNBO), ammonia must be produced using renewable electricity that satisfies stringent criteria for additionality, temporal correlation, and spatial correlation. The electricity may be supplied through a direct connection to an onsite RES power plant or, if drawn from the grid, must be guaranteed by a renewable Power Purchase Agreement (PPA). Until December 31, 2029, temporal correlation must be verified on a monthly basis. However, from 2030 onward, this requirement becomes hourly, necessitating the deployment of energy storage systems to enable continuous 24/7 operation. The only exception applies to bidding zones where the share of renewable electricity exceeded 90% in the previous calendar year. In these zones (highlighted in [Figure S.1 in the Supplementary Material](#)), ammonia production can still be counted as RFNBO, provided that grid electricity consumption does not exceed a maximum number of hours calculated as the total annual hours multiplied by the average renewable share in that bidding zone ([European Commission, 2023b](#)).

Given these criteria, Scenario 1 models an ammonia production plant that fully complies with the EU directive from 2030 for RFNBO production. This results in a RES-based power plant with energy storage, allowing the ammonia production system to operate off-grid, except in zones where the renewable electricity share exceeded 90% in 2024 ([Electricity Maps, 2024](#)), where grid electricity can be purchased. Scenario 2 permits the use of grid electricity without regulatory constraints, allowing for an evaluation of the cost-optimal share of grid electricity, depending on differences in local RES potential and electricity prices. While carbon intensity (Scope 2 emissions accounting both direct and indirect emissions ([Greenhouse Gas Protocol, World Resources Institute, 2025](#))) of ammonia produced in Scenario 1 is considered null, in Scenario 2 it can be assessed based on the electricity carbon intensity of the analysed bidding zone, as detailed in Section 2.2. A scheme of the two scenarios is reported in [Fig. 2](#).

### 2.2. Optimisation approach

A Mixed Integer Linear Programming (MILP) approach is employed to address the cost-optimal sizing and operation of the ammonia production plant. A key challenge in using this method is the linearisation of inherently non-linear features, such as the inclusion of non-constant SOEC efficiency, while minimising the use of auxiliary and binary variables to limit computational time.

The model is implemented in Python and solved using the Gurobi optimisation solver ([Gurobi Optimization, 2025](#)). The decision variables of the optimisation are both component sizes and operation of the plant,

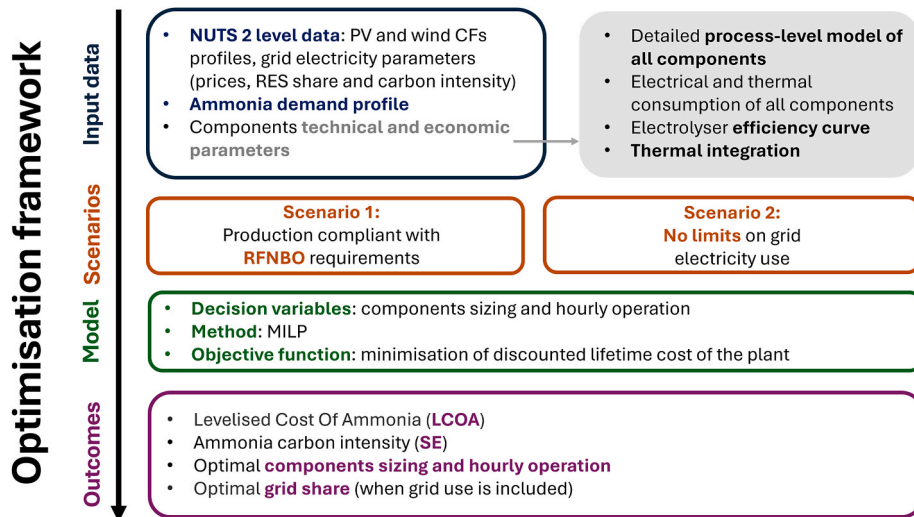


Fig. 1. Optimisation framework of the SOEC-based ammonia production plant.

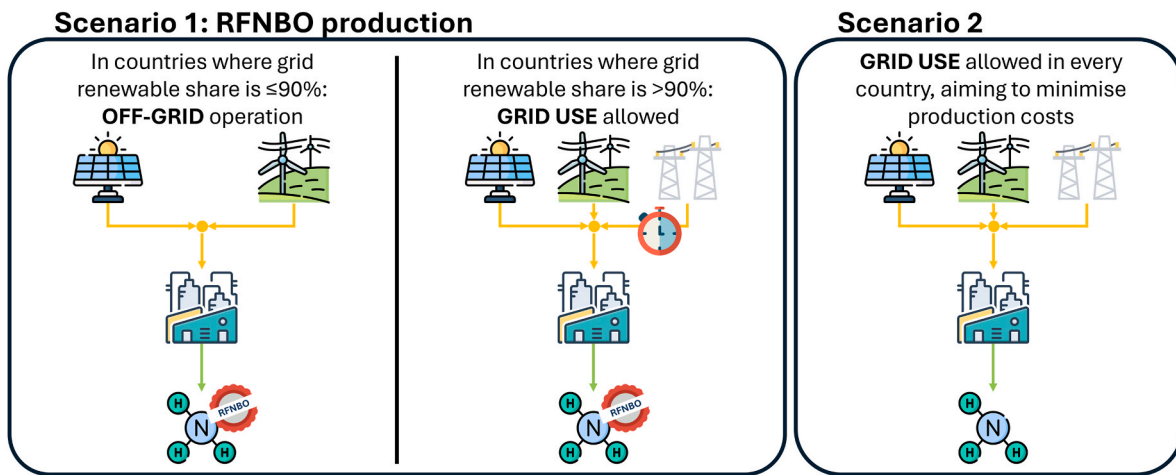


Fig. 2. Overview of the two modelled scenarios. In Scenario 1, the produced ammonia is compliant with the RFNBO European requirements. In Scenario 2, grid electricity can be used without restrictions, and therefore, the produced ammonia does not qualify as RFNBO.

the temporal resolution of 1 h is used, and the model is simulated over a yearly period. The optimisation was solved on a dedicated workstation (Intel Xeon, 32 cores, 128 GB RAM), with the MIPGap constrained to 1%.

The objective function of the optimisation problem is to minimise the discounted lifetime costs ( $C_{tot}$ , in €) of the plant, which include Capital Expenditures (CAPEX), Maintenance and Repair (M&R) costs (accounting for standard annual maintenance and scheduled replacement of specific components), and electricity costs from the grid. The objective function is expressed as follows:

$$C_{tot} = \sum_k I_k + \sum_{y=1}^N \frac{\sum_k M\&R_{k,y}}{(1+d)^y} + \sum_{y=1}^N \frac{E_{grid,y} \cdot C_{grid}}{(1+d)^y} \quad 1$$

where  $I_k$  represents the CAPEX of component  $k$  (in €),  $N$  is the lifetime of the plant (in years),  $M\&R_{k,y}$  is its maintenance and repair cost of component  $k$  in year  $y$  (in €),  $E_{grid,y}$  is the grid electricity consumption in year  $y$  (in kWh),  $C_{grid}$  is the grid electricity price (in €/kWh, according to Eurostat database (Eurostat, 2024)), and  $d$  is the discount rate (in %).

Once all the costs are computed, the Levelised Cost Of Ammonia (LCOA, in €/t<sub>NH3</sub>) is calculated using Eq. (2) (Nayak-Luke and Bañares-Alcántara, 2020):

$$LCOA = \frac{C_{tot}}{\sum_{y=1}^N \frac{M_{NH3,y}}{(1+d)^y}} \quad 2$$

where  $M_{NH3,y}$  is the total ammonia production in year  $y$  (in t)

In Scenario 2, grid share and indirect CO<sub>2</sub> emissions associated with grid electricity usage are also estimated. Grid share is evaluated computing the ratio between the energy purchased from the grid and the total energy consumption of the plant. To capture spatial and temporal variations in emissions, grid carbon intensity is considered on an hourly basis for each bidding zone, according to 2024 data reported by Electricity Maps (Electricity Maps, 2024). Specific Emissions (SE, in tCO<sub>2</sub>/tNH<sub>3</sub>) are evaluated through Eq. (3) (Magnino et al., 2025):

$$SE = \frac{\sum_{t=1}^{8760} E_{grid}(t) \cdot \epsilon_{grid}(t)}{M_{NH3,y}} \quad 3$$

where  $E_{grid}$  is the grid electricity consumption in hour  $h$  (in kWh) and  $\epsilon_{grid}$  is the corresponding grid carbon intensity (in tCO<sub>2</sub>/kWh).

### 2.3. Plant layout

The plant, based on a Haber-Bosch reactor utilising electrolytic H<sub>2</sub>, is composed of the following four main subsystems:

- Electric subsystem: including PV, Wind Turbines (WTs), Battery Energy Storage (BES), and grid connection
- Hydrogen subsystem: comprising SOEC (with its electric heaters) and compressed H<sub>2</sub> storage (including compressor and tank)
- Nitrogen subsystem: consisting of Air Separation Unit (ASU) and N<sub>2</sub> compressor
- Ammonia subsystem: consisting of the HB reactor for NH<sub>3</sub> synthesis

A simplified scheme of the plant layout is shown in Fig. 3, highlighting the key mass, electricity and thermal flows between components.

All the techno-economic parameters of the plant components are summarised in tables in the Supplementary Material, while key economic parameters of the major components are reported in Table 1.

Considering the average size of this type of plants in Europe (SFI, 2023), the rated production of the plant is assumed to be 500,000 t<sub>NH3</sub>/y, while the plant lifetime is set to 25 years (IEA, 2021) (with a discount rate of 4.9% (Marocco et al., 2021)). It is worth noting that plants of this scale require very large electrolyser systems, with rated capacities in the order of 400-700 MW, as detailed in the Supplementary Material, which are substantially larger than currently operating installations (Sunfire, 2025). However, the European Union is strongly promoting the deployment of RFNBOs (European Commission, 2024), making it reasonable to expect that large-scale electrolyser systems (both high- and low-temperature) will be installed in the near future (European Hydrogen Observatory, 2025).

### 2.4. RES potentials

PV and onshore WTs are included as renewable power plants considered in this study. Hourly capacity factors (CFs) for these technologies are obtained from the Copernicus Climate Change Service database, which offers high spatial resolution data starting from 1979 (Copernicus Climate Change Service Climate Data Store, 2020).

Since the energy simulation is conducted on a single-year basis (as described in Section 2.2), a “typical year” is identified for each NUTS 2 region in Europe based on data from 1990 to 2015. The typical year is determined using k-medoids clustering to select a “median year” that minimises mean squared error (all the hourly CFs for each region are

**Table 1**

Major economic parameters of most impacting components. See others on Supplementary Material.

Component	CAPEX	Unit	Ref.
<b>PV</b>			
CAPEX	700	€/kWp	IRENA (2024)
M&R	16	€/(kWp•y)	IRENA (2024)
<b>WT</b>			
CAPEX	1000	€/kW	IRENA (2024)
M&R	3	%CAPEX/year	IRENA (2024)
<b>BES</b>			
CAPEX	250	€/kWh	IRENA (2024)
M&R	3	%CAPEX/year	IRENA (2024)
Lifetime	15	years	Ikaheimo et al. (2018)
<b>SOEC</b>			
CAPEX	2250	€/kW	Böhm et al. (2020)
M&R	4	%CAPEX/year	Nami et al. (2022)
Lifetime	6	years	Zhang et al. (2020)
Replacement cost	23	%CAPEX	Nami et al. (2022)
<b>H<sub>2</sub> Tank</b>			
CAPEX	470	€/kgH <sub>2</sub>	Ikaheimo et al. (2018)
<b>ASU</b>			
CAPEX	1300	€/(kgN <sub>2</sub> /h)	IRENA (2024)
<b>HB</b>			
CAPEX	3400	€/(kgNH <sub>3</sub> /h)	Armijo and Philibert (2020)

reported in the Supplementary Material).

To enable a detailed post-processing analysis of optimal component sizing following the optimisation, which is performed across all NUTS 2 regions, seven representative regions are selected. These are identified by clustering the full set of NUTS 2 regions into seven groups using the k-medoids methodology, based on their mean CFs. Fig. 4 shows the mean normalised CFs for the EU regions and highlights the selected representative regions in red.

### 2.5. Electric subsystem

The electric subsystem is composed of PV system, WTs, BES, and a grid connection. The power drawn from the grid  $P_{grid}$  (in kW) is constrained by an auxiliary variable  $\delta_{grid}$ , which is equal to 1 when grid electricity is purchased and 0 otherwise, as defined in Eq. (4):

$$P_{grid}(t) \leq \delta_{grid}(t) \cdot P_{grid,max} \tag{4}$$

where  $P_{grid,max}$  is the maximum allowable power that can be purchased

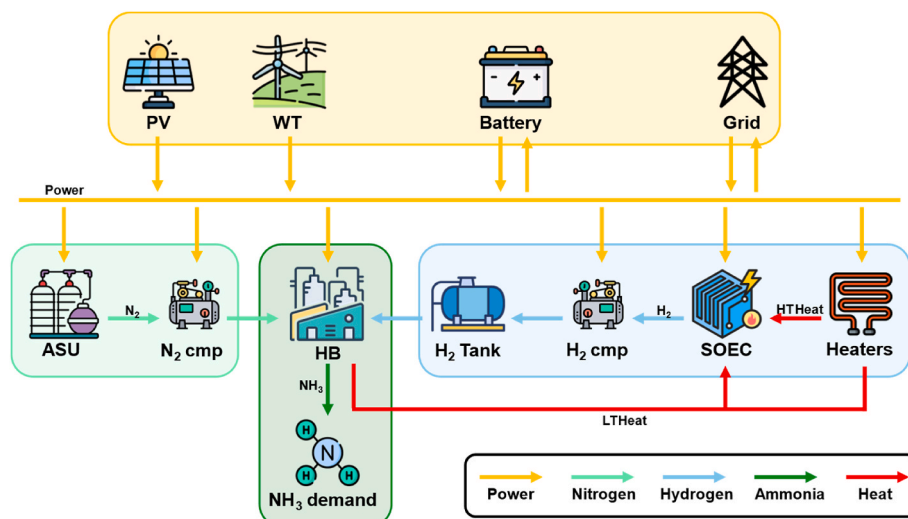


**Fig. 3.** NH<sub>3</sub> production plant layout, highlighting the four subsystems: electricity, hydrogen, nitrogen and ammonia.

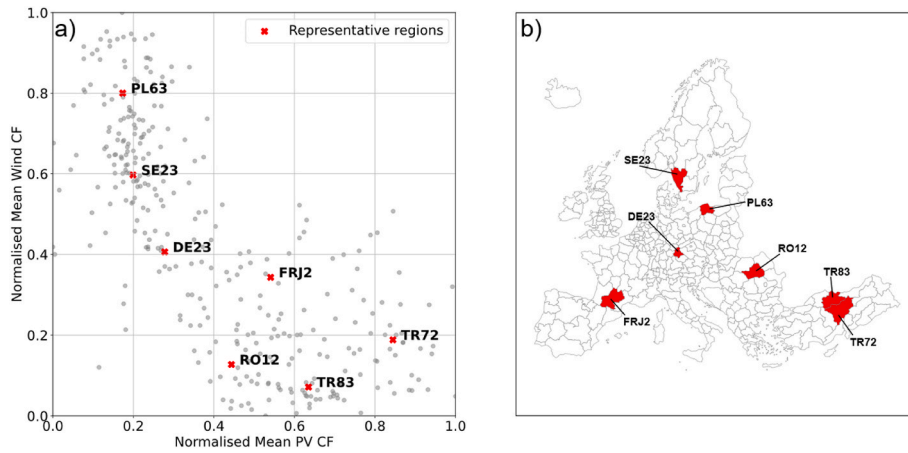


**Fig. 4.** a) Distribution of mean normalised capacity factors (CFs) for PV and WT across all EU regions. Normalization is based on minimum values of 0.003 (WT) and 0.084 (PV), and maximum values of 0.518 (WT) and 0.188 (PV). The 7 representative regions, identified by k-medoids clustering method, are highlighted in red. b) Regions identified in Fig. 4a are highlighted on the map.

from the grid (in kW).

Additionally, in Scenario 1, the number of hours during which electricity can be purchased from the grid is limited depending on the annual renewable share of the grid  $\pi$  (in %) in the corresponding bidding zone in the previous year (see Section 2.1). This constraint is formulated according to Eq. (5):

$$\begin{cases} \sum_{t=1}^{8760} \delta_{grid}(t) \leq \pi \cdot 8760 & \text{if } \pi > 90\% \\ \sum_{t=1}^{8760} \delta_{grid}(t) = 0 & \text{if } \pi \leq 90\% \end{cases} \quad (5)$$

where the value 8760 represents the number of hours in one year, consistent with the annual time horizon adopted in the optimisation.

The power generated by PV and WTs (respectively  $P_{PV}$  and  $P_{WT}$ ) is evaluated at each timestep  $t$  as:

$$P_{PV}(t) = CF_{PV}(t) \cdot P_{PV,r} \quad (6)$$

$$P_{WT}(t) = CF_{WT}(t) \cdot P_{WT,r} \quad (7)$$

where  $CF_{PV}$  and  $CF_{WT}$  are the PV and WT capacity factors, respectively, and  $P_{PV,r}$  and  $P_{WT,r}$  are the corresponding rated powers (in kW).

Given the intrinsic intermittency of renewable energy sources, a lithium-ion (Li-ion) battery is added to the model. At each timestep, the energy stored in the battery  $E_{BES}$  (in kWh) is evaluated using Eq. (8) (Marocco et al., 2026):

$$E_{BES}(t) = E_{BES}(t-1) \cdot (1 - \sigma_{bt}) + P_{BES,ch}(t-1) \cdot \Delta t \cdot \eta_{BES,ch} - P_{BES,dis}(t-1) \cdot \frac{\Delta t}{\eta_{BES,dis}} \quad (8)$$

where  $\sigma_{bt}$  is the battery self-discharge coefficient,  $P_{BES,ch}$  and  $P_{BES,dis}$  are the charging and discharging powers (in kW),  $\eta_{BES,ch}$  and  $\eta_{BES,dis}$  are the corresponding efficiencies, and  $\Delta t$  the time step (set to 1 h).

The power balance at the electric bus is formulated as in Eq. (9):

$$\begin{aligned} P_{PV}(t) + P_{WT}(t) + P_{BES,dis}(t) + P_{grid}(t) &= P_{BES,ch}(t) + P_{exc}(t) + P_{EL}(t) \\ &+ P_{heat}(t) + P_{ASU}(t) + P_{HC}(t) \\ &+ P_{NC}(t) + P_{HB}(t) \end{aligned} \quad (9)$$

where  $P_{grid}$  is the power purchased from the grid (in kW),  $P_{exc}$  is the excess power (in kW) (no remuneration is assumed for this energy),  $P_{EL}$  is the power supplied to the electrolyser system (in kW, including stack, balance of plant, and high temperature heaters, but excluding heat required for warm stand-by),  $P_{ASU}$  is the power demand of the ASU (in kW),  $P_{HC}$  is the power consumed by the  $H_2$  compressor (in kW),  $P_{NC}$  is

the power consumed by the  $N_2$  compressor (in kW),  $P_{HB}$  is the power demand of the HB process (in kW), and  $P_{heat}$  (in kW) is defined as:

$$P_{heat}(t) = H_{in,low}(t) + H_{in,sth}(t) \quad (10)$$

where  $H_{in,low}$  is the low-temperature heat for steam generation inside the SOEC system (in kW) and  $H_{in,sth}$  is the high-temperature heat for SOEC warm stand-by (in kW, see Section 2.6 for details).

## 2.6. Hydrogen subsystem

The hydrogen subsystem comprises a SOEC system (layout shown in Fig. 5), along with an  $H_2$  compressor, an  $H_2$  storage tank, and electric heaters. Compared to low-temperature electrolysers, the SOEC technology offers higher conversion efficiency (Luo et al., 2014), making it a cost-effective option for integration with ammonia production, despite its higher capital costs. A key limitation of SOEC technology lies in its high operating temperature, typically between 700 °C and 900 °C.

Since SOECs commonly operate at or below the thermoneutral point (Wolf et al., 2023), additional thermal energy is needed to sustain the electrolysis process. In this analysis, a modest temperature drop ( $\sim 20$  °C) across the flows entering and exiting the stack is assumed to account for this energy input.

To prevent cell degradation, the feedwater must be vaporised and preheated prior to entering the SOEC stack, necessitating an external heat supply. In this model, the SOEC thermal requirements are explicitly split into low-temperature (LT) heat for steam generation (water/steam around 100 °C) and high-temperature (HT) heat for reactant preheating up to the stack inlet temperature ( $\sim 800$  °C) and for warm stand-by. Part of the LT heat demand (LT Heat in Fig. 5) is met by recovering waste heat from the exothermic ammonia synthesis. The available hot stream is assumed at approximately 400 °C, providing a sufficient driving force for steam generation, so that temperature feasibility does not represent a limiting factor for this LT heat integration. Conversely, the temperature of the recovered waste heat is insufficient to raise the reactant streams to the required stack inlet temperature, which must closely match the stack's operating temperature to prevent thermal stress and potential damage. Therefore, high-temperature electric heaters are also included to supply the remaining heat needed to achieve the necessary inlet conditions (HT Heat in Fig. 5).

The SOEC considered in this analysis is based on the model tested by Hauch et al. (2020), and consists of a fuel electrode made of Ni/3YSZ, an LSC oxygen electrode, and an 8YSZ electrolyte layer, operating at 800 °C. To accurately simulate SOEC performance, particularly under partial-load conditions and considering its non-linear behaviour, an

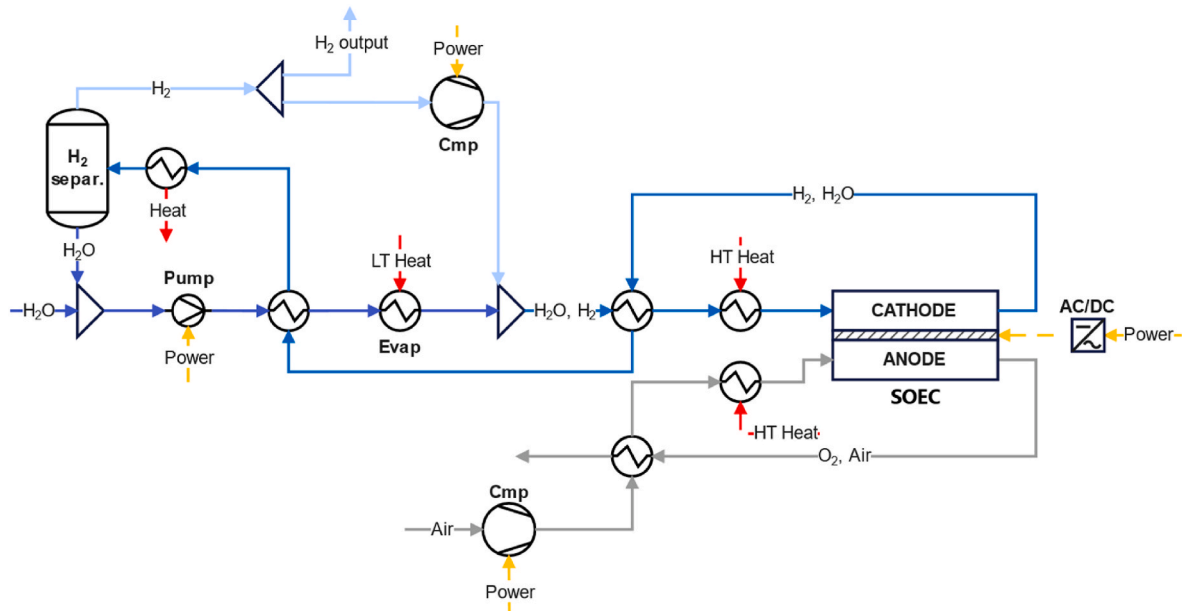


**Fig. 5.** SOEC system layout. “LT Heat” refers to the low-temperature heat supplied to the steam generator. This heat is partially recovered by the exothermic HB reactors, with the remainder provided by low-temperature electric heaters. “HT Heat” denotes the high-temperature heat necessary to raise the inlet streams to the SOEC stack temperature. High-temperature heaters are also used during warm stand-by period.

efficiency curve is incorporated into the model (“Electrical-only + HT heater” in Fig. 6). A piecewise linear approximation of the SOEC performance curve is implemented, enabling an accurate representation of SOEC operation while maintaining the linearity of the optimisation problem. Additional details regarding the SOEC modelling and its piecewise linear approximation are provided in the Supplementary Material.

The SOEC is assumed to operate within a load range of 25% to 100% of the nominal power (Schwarze et al., 2023). To implement this operational constraint while still allowing for periods of inactivity, an auxiliary variable ( $P_{EL,r,aux}$ ) is introduced:

$$P_{EL,r,aux} = P_{EL,r} \cdot \delta_{EL}(t) \quad 11$$

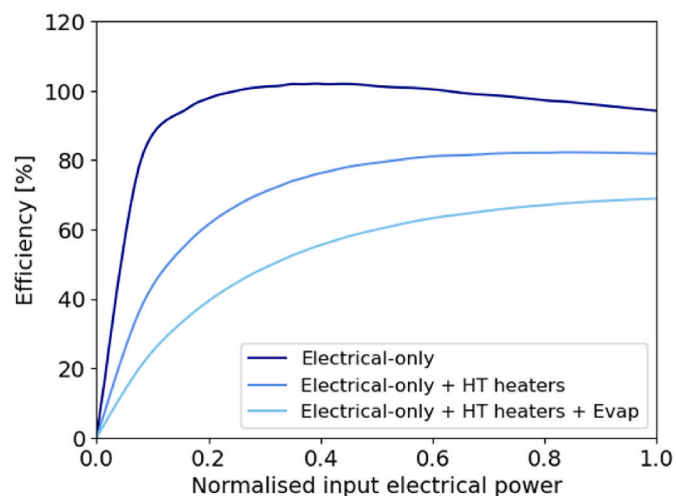


**Fig. 6.** SOEC system efficiency curve. “Electrical-only” accounts for all electrical consumption within the system, including both the electrolyser stack and BOP, but excludes heat demand. “Electrical-only + HT heaters” includes all electrical consumption, also encompassing high-temperature heaters. “Electrical-only + HT heaters + Evap” accounts for both electrical consumption and the thermal energy needed for steam generation (without considering thermal integration with the HB process).

where  $P_{EL,r}$  (in kW) is the rated electrical power of the SOEC, and  $\delta_{EL}$  is a binary variable used to express whether the SOEC is operating ( $\delta_{EL} = 1$ ) or not ( $\delta_{EL} = 0$ ). To preserve linearity within the MILP-based model, this equation cannot be directly implemented in its current form. Instead, it must be reformulated into a set of linear inequalities, as described in Marocco et al. (2021) and detailed further in the Supplementary Material.

SOECs are particularly sensitive to shutdowns, which can accelerate cell degradation and reduce system longevity (Hanasaki et al., 2014). Moreover, resorting to a full cold shutdown would entail several hours of heating before resuming operation (Danish Energy Agency, 2016), in order to avoid damaging the cells. To mitigate this, the electrolyser is generally kept at high temperatures during idle periods, a condition referred to as “warm stand-by”. This mode requires a heat demand, which is supplied by electric heaters and is estimated to be 5.5% of the nominal SOEC power (Schwarze et al., 2023). Maintaining the cell at high temperatures significantly reduces ramp-up times, which are reported to be approximately 10% of nominal load per minute (Sunfire, 2024). Given the model’s hourly timestep, this parameter is considered negligible.

Downstream of the SOEC, an H<sub>2</sub> compressor and H<sub>2</sub> tank are included, whose operation is described through the following equations:

$$P_{HC}(t) = SEC_{HC} \cdot G_{H,EL}(t) \quad 12$$

$$M_{H,HT}(t) = M_{H,HT}(t-1) + G_{H,HC}(t-1) \cdot \Delta t \cdot \eta_{HT,ch} - G_{H,HB}(t-1) \cdot \frac{\Delta t}{\eta_{HT,dis}} \quad 13$$

where  $SEC_{HC}$  is the specific electricity consumption of the H<sub>2</sub> compressor (in kWh/kg<sub>H<sub>2</sub></sub>),  $G_{H,HC}$  is the H<sub>2</sub> mass flow rate through the compressor and exiting the SOEC (in kg/h),  $M_{H,HT}$  is the H<sub>2</sub> stored in the hydrogen tank (in kg), and  $G_{H,HB}$  is the mass flow rate of H<sub>2</sub> entering the HB reactor (in kg/h). The terms  $\eta_{HT,ch}$  and  $\eta_{HT,dis}$  correspond to the charging and discharging efficiencies of the H<sub>2</sub> tank to account for leakage losses.

### 2.7. Nitrogen subsystem

The nitrogen subsystem consists of the ASU and the N<sub>2</sub> compressor. Given the large scale of the plant and the high purity of N<sub>2</sub> required for

the process (Yoshida et al., 2021), a two-column cryogenic distillation is assumed, which is characterised by relatively low energy consumption. To supply the HB reactor with nitrogen at the required pressure, a compressor with an outlet pressure of 350 bar is included. The power consumption of the ASU and N<sub>2</sub> compressor ( $P_{ASU}$  and  $P_{NC}$ ) is evaluated as follows:

$$P_{ASU}(t) = SEC_{ASU} \cdot G_{N,ASU}(t) \quad 14$$

$$P_{NC}(t) = SEC_{NC} \cdot G_{N,ASU}(t) \quad 15$$

where  $G_{N,ASU}$  is the N<sub>2</sub> mass flow rate from the ASU (in kg/h), while  $SEC_{ASU}$  and  $SEC_{NC}$  are the Specific Electricity Consumption (SEC) of the ASU and nitrogen compressor, respectively (in kWh/kg<sub>N<sub>2</sub></sub>).

## 2.8. Ammonia subsystem

The ammonia subsystem is primarily composed of the HB reactor. The ammonia synthesis reaction is exothermic, and the reactor generates excess heat at approximately 400 °C, which can be recovered and used in the SOEC to supply LT heat for steam generation. Since the HB process is preceded by a high-pressure H<sub>2</sub> tank and a nitrogen compressor, its electrical consumption is relatively low, being mainly associated with the compressor used to recirculate unreacted gases (Magnino et al., 2025). Due to the use of catalysts, the HB process has limited operational flexibility and is particularly sensitive to shutdowns. However, these characteristics make it well-suited for integration with SOECs, which exhibit similar operational constraints. The operation of HB reactor is described by the following equations:

$$P_{HB}(t) = SEC_{HB} \cdot G_{A,HB}(t) \quad 16$$

$$y_{min,HB} \cdot G_{A,HB,r} \leq G_{A,HB}(t) \leq y_{max,HB} \cdot G_{A,HB,r} \quad 17$$

where  $SEC_{HB}$  is the specific electricity consumption of the HB (in kWh/kg<sub>NH<sub>3</sub></sub>),  $G_{A,HB}$  is the ammonia mass flow rate from the HB system (in kg/h),  $y_{min,HB}$  and  $y_{max,HB}$  are the minimum and the maximum load of the HB respectively (80% and 100% of the nominal capacity respectively (Salmon and Bañares-Alcántara, 2021)), and  $G_{A,HB,r}$  is the nominal production capacity of HB system (in kg/h).

Considering that the thermal energy from the exothermic reaction can offset part of the heat demand of the SOEC (as described in Section 2.6), Eq. (18) is included to represent this thermal integration:

$$H_{in,low}(t) \geq SHD_{EL} \cdot P_{EL,r,aux}(t) - SHP_{HB} \cdot G_{A,HB}(t) \quad 18$$

where  $H_{in,low}$  is the low-temperature heat provided by the electric heater associated with the SOEC (in kW, see Eq. (10)),  $SHD_{EL}$  is the low-temperature Specific Heat Demand (SHD) of the SOEC (in kW<sub>th</sub>/kW<sub>el</sub>),  $P_{EL,r,aux}$  is the auxiliary variable related to the SOEC rated power and its state of operation (see Section 2.6), and  $SHP_{HB}$  is the Specific Heat Produced (SHP) by the HB process (in kW/kg<sub>NH<sub>3</sub></sub>). The inequality sign in Eq. (18) is set to permit  $H_{in,low}$  to be zero when the electrolyser is not in operation.

## 3. Results

The LCOA results for the various regions under the two scenarios are presented in Sections 3.1 and 3.2, respectively. Then, Section 3.3 provides insights into the different plant configurations.

### 3.1. Scenario 1

This section presents the LCOA values across EU regions under Scenario 1 (RFNBO production), where electricity is supplied by on-site PV and WT systems, except in bidding zones where the annual renewable share of electricity exceeded 90% in 2024, ensuring compliance with DR

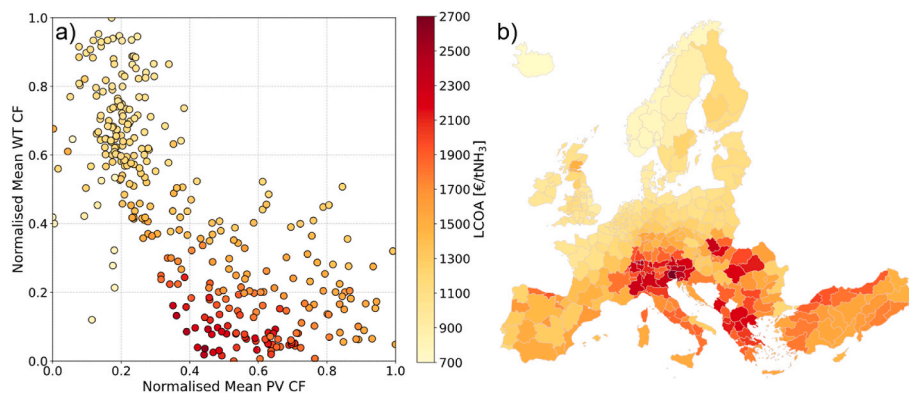
2023/1184 (European Commission, 2023b).

Fig. 7a displays a heatmap of the resulting LCOA values, with each dot representing a NUTS 2 region. The coordinates of each dot are based on the corresponding normalised mean capacity factors for PV and WT. Across the analysed regions, LCOA values range from approximately 770 to 2600 €/tNH<sub>3</sub>. These findings align well with previous studies in the literature (Campion et al., 2023; IEA, 2023; Sousa et al., 2022), although they remain significantly higher than those associated with SMR-based ammonia production, typically in the range of 250 to 1000 €/tNH<sub>3</sub> (IEA, 2023).

An analysis of the colour distribution in Fig. 7a highlights that the mean WT CF is the primary determinant of LCOA variability. Regions with higher WT CFs exhibit lower LCOA values, with the upper-left corner of the plot characterised by yellow dots. In contrast, the impact of PV on reducing LCOA is less pronounced compared to WT. This trend emphasises the critical role of wind resources in reducing the cost of ammonia production. This behaviour can be explained by both mean CFs and temporal matching effects. First, WT CFs display a wider regional spread (varying between 0 and 0.5 on an annual basis) than PV (ranging from 0.08 to 0.19), which amplifies the impact of wind resource quality on optimal sizing and costs. Second, a non-negligible share of the electricity demand of the SOEC-HB system is continuous over 24 h, since the HB reactor is constrained to operate between 80% and 100% of nominal capacity and the SOEC also maintains auxiliary consumption and warm stand-by heat demand during idle periods. Under such operating constraints, PV generation is intrinsically penalised by its deterministic day-night cycle, which forces either important renewable oversizing or larger storage systems to ensure continuity of supply during non-generating hours. Conversely, wind generation typically exhibits a higher share of useable production hours and can better align with the near-baseload electricity demand, lowering LCOA. While PV still provides a secondary benefit in regions with high solar potential by complementing wind generation, its lower CF and diurnal intermittency limit the achievable LCOA reductions compared to wind-dominated regions. Consistent with this, previous studies show that PV-driven ammonia plants require substantially higher installed generation capacity and achieve lower electrolyser utilisation than wind-driven sites, whereas hybrid PV-WT configurations can reduce storage needs by exploiting profile complementarity (Bose et al., 2022; Wang et al., 2023). This can be further observed in the cost breakdown provided in Section 3.3, where renewable generation capacity and storage dominate total costs, making the LCOA highly sensitive to resources that maximise annual energy yield and useable production hours. Additional evidence is provided in the Supplementary Material, where the correlation between LCOA and PV and WT CFs is further analysed. At the same time, it should be noted that the relative advantage of wind versus PV is not universal and depends on regional resource distributions and demand constraints. Other studies have reached different results at global level (Fasihi et al., 2021), which can be justified considering that the European regions with the strongest wind resources are also among the most favourable globally (Davis et al., 2023), whereas the regions with the highest solar potential are generally located at lower latitudes (such as the Northern Sahara and Arabic Peninsula (SolargisWorld Bank Group, 2025)).

Finally, some regions located towards the lower-left corner of the plot of Fig. 7a exhibit very low LCOA values, despite having lower CFs compared to other areas in Europe. These correspond to regions in Norway, where grid electricity usage is permitted due to the high share of renewable energy produced in 2024 (between 92% and 99% depending on the bidding zone), primarily from hydropower (Electricity Maps, 2024). Access to low-cost grid electricity helps keep LCOAs very low in these regions, whereas a fully off-grid scenario would result in significantly higher ammonia production costs.

Fig. 7b shows the same LCOA data on a map of Europe. Except for Norway, Iceland, and northern Sweden (which benefit from grid use since renewable share exceeded 90% in 2024), the most competitive



**Fig. 7.** Scenario 1: a) Heatmap of LCOA values [€/tNH<sub>3</sub>] across EU NUTS 2 regions as a function of normalised mean CFs for PV and WT. Normalization is based on minimum values of 0.003 (WT) and 0.084 (PV), and maximum values of 0.518 (WT) and 0.188 (PV), b) Heatmap of LCOA values [€/tNH<sub>3</sub>] across European regions in Scenario 1 (off-grid scenario).

regions are those bordering the English Channel, North Sea, and Baltic Sea, where wind potential is higher. These regions exhibit the lowest LCOA values, reinforcing the critical role of wind resources in reducing ammonia production costs. In contrast, regions with strong solar potential but relatively weak wind resources, such as Greece and Turkey, show higher LCOA values. The least favourable areas in Scenario 1 are northern Italy, Switzerland, Austria, and Slovenia. These regions, characterised by relatively low renewable energy potential for both PV and wind, face significantly higher investment requirements for renewable energy systems. Consequently, ammonia production in these regions is considerably more expensive, with LCOA values among the highest in the analysis.

This spatial distribution highlights the importance of optimising plant siting based on renewable resource availability, given its strong impact on economic feasibility.

### 3.2. Scenario 2

Scenario 2 allows grid electricity, with the optimal grid share determined endogenously by cost minimisation. Fig. 8a presents a European heatmap of LCOA values under this setting, where grid electricity prices (Eurostat, 2024) influence ammonia costs. The regional ranking remains broadly consistent with Scenario 1: the windiest regions, such as northern France, England, Denmark, and northern Poland, continue to be the most cost-competitive. Additionally, Turkey and Scandinavian countries also emerge as low-cost regions. Conversely, Italy and central Europe continue to exhibit higher LCOA values. However, the inclusion of grid electricity reduces LCOA values across all regions, offering an additional degree of flexibility. The LCOA range narrows significantly in Scenario 2, from 730 to 1600 €/tNH<sub>3</sub>, with the reduction particularly pronounced in regions that recorded the highest costs in Scenario 1.

Fig. 8b shows the share of grid electricity in the total plant electricity consumption under Scenario 2. The reliance on grid electricity varies significantly across Europe, driven by the renewable potential and grid electricity prices in each region. In Southern Europe, grid shares are typically 50–70%. Iceland and Scandinavia also display high reliance, with Norway approaching ~100%, whereas Poland, Germany, the UK, and Ireland rely on the grid for <15%, thanks to strong wind resources that outcompete grid electricity.

The underlying reasons for low grid electricity prices differ across regions. In Norway and Iceland, grid electricity is predominantly renewable, sourced from hydro and geothermal resources (Electricity Maps, 2024). Therefore, relying on grid electricity is not a concern in terms of environmental impact, since the level of decarbonisation achieved by these grids is already advanced. On the other hand, in Turkey, Italy, and Balkan countries, grid electricity prices are kept low by the significant use of coal and natural gas (Electricity Maps, 2024), leading

to a higher optimal grid share in Scenario 2. This would reduce the optimal share of grid electricity in similar scenarios, potentially shifting the cost dynamics observed in Scenario 2.

Fig. 8c presents the ammonia carbon intensity (in tCO<sub>2</sub>/tNH<sub>3</sub>) under Scenario 2, calculated based on the hourly profiles of grid electricity carbon intensity (Electricity Maps, 2024). It can be observed that, in countries with a high share of renewable energy, such as Sweden and Norway, the high grid reliance reported in Fig. 8b does not translate into carbon-intensive ammonia production. Conversely, in Turkey and Balkans, where electricity generation is heavily reliant on fossil fuels (Electricity Maps, 2024), the resulting ammonia exhibits a high carbon intensity, even exceeding the values of fossil-based ammonia, which typically range from 1.9 to 2.5 tCO<sub>2</sub>/tNH<sub>3</sub> (McKinsey, 2023).

### 3.3. Optimal sizing ratios

In this section, a detailed analysis of the cost composition contributing to the LCOA is presented, along with an evaluation of component sizing. Seven representative regions across Europe, as outlined in Section 2.4, are used for this purpose.

Fig. 9 illustrates the cost breakdown for the ammonia production plants in the seven representative regions under both scenarios (detailed data are also provided in the Supplementary Material). In Scenario 1, renewable energy generators, which includes PV panels and WTs, accounts for approximately 50% of the total plant costs across all regions. In Scenario 2, this share decreases due to increased reliance on electricity purchased from the grid. The relative contributions of PV and WTs vary depending on the renewable potential of each region. For example, sun-rich regions, such as those in Turkey (TR72 and TR83), exhibit higher costs associated with PV systems, while in wind-abundant regions like PL63, the costs are predominantly shifted towards WTs. In Scenario 2, where grid electricity is utilised, the cost of purchasing grid electricity can constitute up to about 60% of the total (as in RO12), particularly in regions where on-site renewable generation is less feasible. Conversely, energy storage systems, including BES and H<sub>2</sub> tanks, which are significant cost components in Scenario 1, are largely unnecessary in Scenario 2, particularly in wind-dominated areas. The electrolyser also shows a reduction in size when transitioning from Scenario 1 to Scenario 2, yet it remains a significant cost driver in both scenarios. Other plant components – such as the H<sub>2</sub> compressor, air separation unit, N<sub>2</sub> compressor, and Haber-Bosch reactor – contribute only marginally to the overall costs.

Fig. 10 presents the autonomies (hours) of the two storage systems, BES and H<sub>2</sub> tank, defined as capacity divided by the relevant output flow (electrical power for the BES, hydrogen flow for the tank) required to keep the plant operational and meet the average hourly NH<sub>3</sub> production demand. The x- and y-axes show the normalised mean CFs for PV and

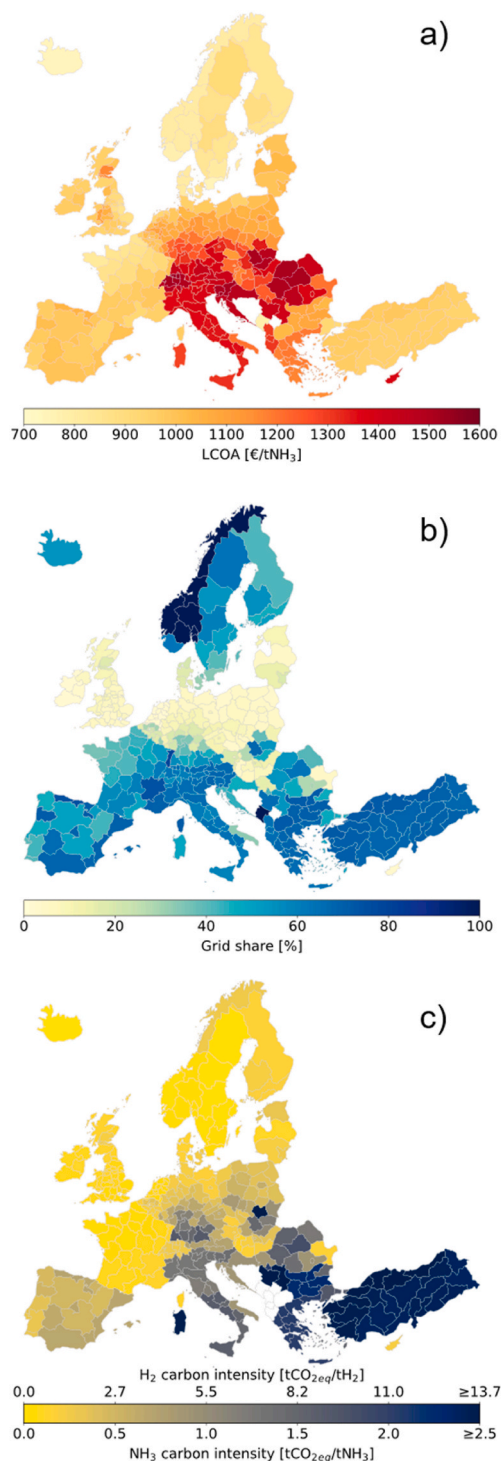


**Fig. 8.** Scenario 2: a) Heatmap of LCOA values [€/tNH<sub>3</sub>] across European regions, b) Share of grid electricity in the total plant electricity consumption across European regions, c) NH<sub>3</sub> and H<sub>2</sub> carbon intensity [tCO<sub>2eq</sub>/tNH<sub>3</sub> and tCO<sub>2eq</sub>/tH<sub>2</sub>] across European regions (calculated based on the local electricity grid carbon intensity). White areas indicate regions for which no publicly available data on grid carbon intensity are available.

WTs, respectively.

In Fig. 10a (Scenario 1), a clear pattern emerges: in wind-rich regions, battery autonomy is limited to a few hours because wind provides a relatively steady contribution over the year and better sustains the plant's minimum loads (e.g., HB recirculation and SOEC warm standby). Where WT CFs are low, larger batteries are required to cover

night-time and overcast periods; the need is particularly acute in PV-dominated areas, where intra-day variability is pronounced. Fig. 10b shows that, in Scenario 1, H<sub>2</sub> tanks typically achieve substantially higher autonomies than batteries, ranging from 50 to 300 h in most regions, with peaks reaching 700 h. This reflects the storage requirements arising from the SOEC optimisation strategy, which necessitates a flexible hydrogen buffer to balance production and demand.

In Scenario 2 (Fig. 10c and d), storage systems disappear in most of the regions (respectively 232 for BES and 195 for H<sub>2</sub> tanks, out of 334 regions), because the grid more economically guarantees continuity for fixed minimum loads. However, in less favourable regions, storage systems remain necessary, with H<sub>2</sub> tank autonomies reaching up to 60 h.

Fig. 11 presents the share of surplus electricity in the system, defined as the ratio of excess electricity to total renewable generation. In Scenario 1, the highest surplus shares occur in regions dominated by solar resources, where the required oversizing of PV capacity leads to substantial excess electricity generation. Conversely, regions with more balanced CFs between PV and WT tend to exhibit lower levels of surplus energy. Notably, in some regions, the share of excess energy reaches up to 50%. This suggests that, if such excess energy were exported to the grid and associated revenues were considered, overall plant costs could potentially be reduced compared to the results shown in earlier sections. However, this potential revenue was intentionally excluded from the study to maintain the focus on a 'pure' ammonia production plant rather than a power producer. This approach ensures that the optimisation process remains aligned with the goal of minimising ammonia production costs, without incentivising the oversizing of generation capacity for the purpose of selling electricity to the grid.

In Scenario 2, surplus shares are significantly lower, as the presence of grid electricity enables a downsizing of both PV and WT systems, thereby limiting excess generation and associated curtailment or grid exports.

#### 4. Conclusions

This study investigates the optimal design of ammonia production plants based on Solid Oxide Electrolyser Cell (SOEC) technology across Europe. A Mixed Integer Linear Programming (MILP) approach is employed with the objective of minimising production costs. The optimisation framework models energy consumption and mass balances for all components, together with heat integration between the Haber-Bosch (HB) and electrolysis systems to reduce overall energy use. Additionally, the model incorporates SOEC thermal requirements during warm-standby periods and an efficiency curve to accurately represent part-load performance.

The analysis covers all European NUTS 2 regions to evaluate the cost-competitiveness of electrolytic ammonia production, accounting for regional variations in renewable energy potential and grid characteristics. Two main scenarios are considered to assess the impact of the Renewable Energy Directive (RED III) requirements on production costs and components sizing:

- Scenario 1: the ammonia production plant is assumed to operate off-grid, supplied exclusively by photovoltaic (PV) and wind turbines (WTs), except in regions where the annual share of renewable electricity exceeded 90% of the total production in 2024. In Scenario 1, ammonia qualifies as Renewable Fuel of Non-Biological Origin (RFNBO).
- Scenario 2: no limits are imposed on grid electricity usage, with the sole objective of minimising production costs.

As for Scenario 1, regions with strong wind resources, such as Denmark, England, and Poland, generally achieve lower Levelised Cost Of Ammonia (LCOA) values, ranging between 800 and 1000 €/tNH<sub>3</sub>. Indeed, wind power, although variable, tends to exhibit smooth fluctuations over time, effectively matching the continuous consumption

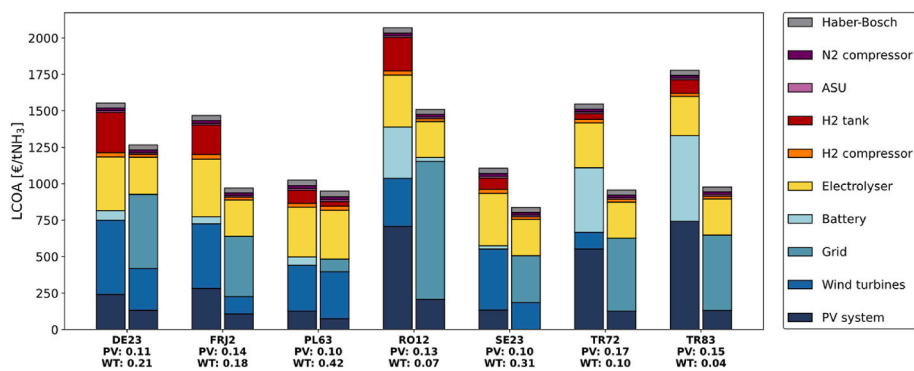


Fig. 9. Cost breakdown of NH<sub>3</sub> production plant in the seven representative regions: for each region, the first column corresponds to Scenario 1 and the second to Scenario 2. The x-axis labels indicate the region names along with their respective average CFs for PV and WT.

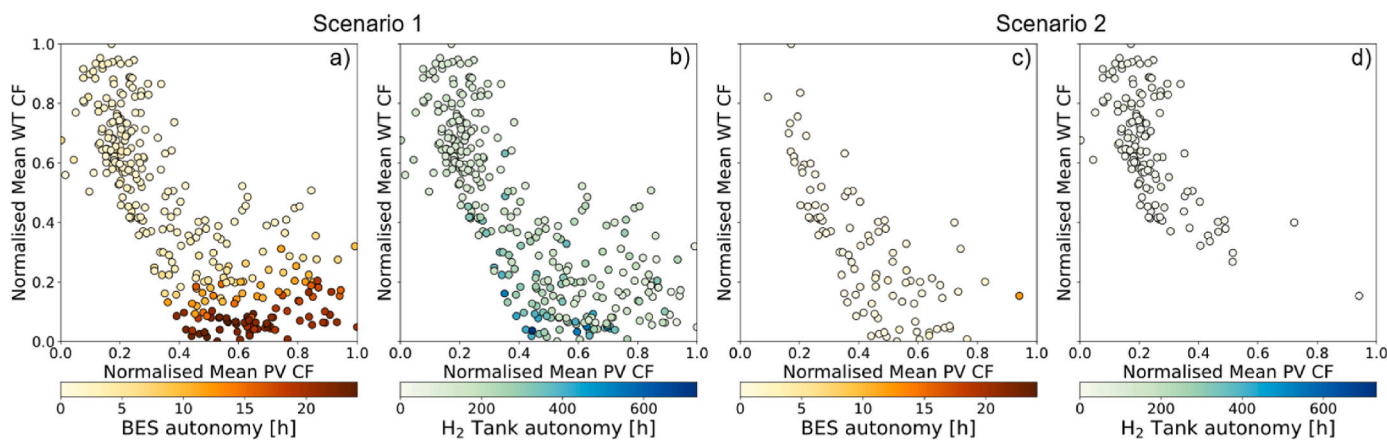


Fig. 10. Heatmap of BES and H<sub>2</sub> tank autonomies (in h) for Scenario 1 and Scenario 2. Colour intensity represents the autonomy duration. The axes display the normalised mean CFs for PV and WT. Normalization is based on the following extrema: for PV, a minimum of 0.084 and a maximum of 0.188; for WT, a minimum of 0.003 and a maximum of 0.518. (For interpretation of the references to colour in this figure legend, the reader is referred to the Web version of this article.)

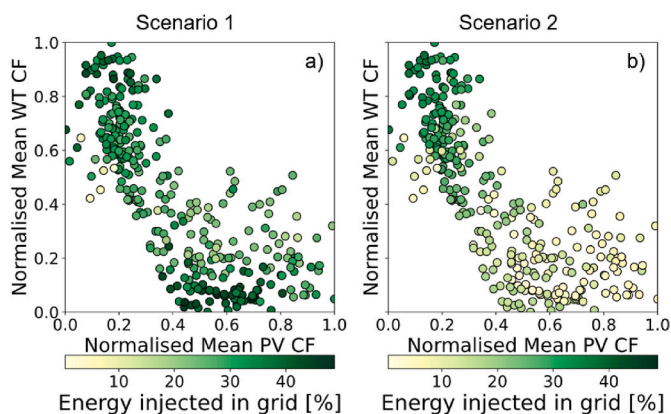


Fig. 11. Heatmap of the electrical energy injected into the grid, reported as share of the total energy produced by the renewable generation plant for Scenario 1 and Scenario 2. Colour intensity represents the shares. The axes display the normalised mean CFs for PV and WT. Normalization is based on the following extrema: for PV, a minimum of 0.084 and a maximum of 0.188; for WT, a minimum of 0.003 and a maximum of 0.518. (For interpretation of the references to colour in this figure legend, the reader is referred to the Web version of this article.)

requirements of the Haber-Bosch and SOEC processes. By contrast, solar-dominated regions are less competitive (exceeding 2000 €/tNH<sub>3</sub>), due to the need for large energy storage systems to cover nights and cloudy

days. In particular, regions with limited wind resources require extensive batteries and hydrogen storage capacities, on the order of around 20 and 300 h of autonomy, respectively. In wind-rich areas, these requirements are markedly reduced, to about 2 and 60 h for batteries and H<sub>2</sub> storage.

In Scenario 2, where unrestricted use of grid electricity is allowed, LCOA values are substantially reduced in regions characterised by low renewable energy potential and favourable grid electricity prices. However, depending on the grid carbon intensity in each bidding zone, reliance on grid electricity can lead to high indirect emissions associated with ammonia production, as observed in Turkey, the Balkans, and Italy.

The proposed optimisation framework can be readily adapted to investigate hybrid configurations, both in terms of power supply (e.g., offshore wind, hydropower, or nuclear) and hydrogen conversion technologies (e.g., hybridisation of low- and high-temperature electrolysis). While this work focuses on RFNBO-compliant ammonia production under RED III, the regulatory layer can be treated as scenario-dependent, enabling the implementation of alternative constraints reflecting other geopolitical contexts or less stringent requirements to assess economic feasibility under partial decarbonisation scenarios. Finally, as European energy and hydrogen regulations continue to evolve, it is important that cost assessments remain aligned with the most recent regulatory frameworks.

**CRedit authorship contribution statement**

**Alessandro Magnino:** Writing – original draft, Visualization, Software, Resources, Methodology, Investigation, Formal analysis, Data

curation, Conceptualization. **Paolo Marocco**: Writing – review & editing, Visualization, Validation, Supervision, Project administration, Methodology, Conceptualization. **Massimo Santarelli**: Writing – review & editing, Supervision. **Marta Gandiglio**: Writing – review & editing, Visualization, Validation, Supervision, Project administration, Methodology, Funding acquisition, Conceptualization.

### Declaration of competing interest

The authors declare that they have no known competing financial interests or personal relationships that could have appeared to influence the work reported in this paper.

### Acknowledgements

The work has been conducted in the framework of the AMPS (Automated Mass Production of SOC Stack) project (<https://www.amps-project.eu/>). The project is supported by the Clean Hydrogen Partnership and its members (GA: 101111882).

Project funded under the National Recovery and Resilience Plan (NRRP), Mission 4. Component 2 Investment 1.3 - Call for tender No. 1561 of October 11, 2022 of Ministero dell'Università e della Ricerca (MUR); funded by the European Union – NextGenerationEU. Project code PE0000021, Concession Decree No. 1561 of October 11, 2022 adopted by Ministero dell'Università e della Ricerca (MUR), CUP - E13C22001890001, Project title "Network 4 Energy Sustainable Transition – NEST".

### Appendix A. Supplementary data

Supplementary data to this article can be found online at <https://doi.org/10.1016/j.jclepro.2026.148079>.

### Data availability

Data will be made available on request.

### References

- Armijo, J., Philibert, C., 2020. Flexible production of green hydrogen and ammonia from variable solar and wind energy: case study of Chile and Argentina. *Int. J. Hydrogen Energy* 45, 1541–1558. <https://doi.org/10.1016/j.ijhydene.2019.11.028>.
- Böhm, H., Zauner, A., Rosenfeld, D.C., Tichler, R., 2020. Projecting cost development for future large-scale power-to-gas implementations by scaling effects. *Appl. Energy* 264, 114780. <https://doi.org/10.1016/j.apenergy.2020.114780>.
- Bose, A., Lazouski, N., Gala, M.L., Manthiram, K., Mallapragada, D.S., 2022. Spatial variation in cost of electricity-driven continuous ammonia production in the United States. *ACS Sustain. Chem. Eng.* 10, 7862–7872. <https://doi.org/10.1021/ACSUSCHEMENG.1C08032>.
- Campion, N., Nami, H., Swisher, P.R., Vang Hendriksen, P., Münster, M., 2023. Techno-economic assessment of green ammonia production with different wind and solar potentials. *Renew. Sustain. Energy Rev.* 173, 113057. <https://doi.org/10.1016/j.rser.2022.113057>.
- Cinti, G., Frattini, D., Jannelli, E., Desideri, U., Bidini, G., 2017. Coupling solid oxide electrolyser (SOE) and ammonia production plant. *Appl. Energy* 192, 466–476. <https://doi.org/10.1016/j.apenergy.2016.09.026>.
- Copernicus Climate Change Service (C3S), Climate Data Store (CDS), 2020. Climate and Energy Indicators for Europe from 1979 to Present Derived from Reanalysis. <https://doi.org/10.24381/cds.4bd77450> [WWW Document].
- Danish Energy Agency, 2016. Renewable fuels - technology descriptions and projections for long-term energy system planning [WWW Document]. URL: <https://ens.dk/en/analyses-and-statistics/technology-data-renewable-fuels>.
- Davis, N.N., Badger, J., Hammann, A.N., Hansen, B.O., Mortensen, N.G., Kelly, M., Larsén, X.G., Olsen, B.T., Floors, R., Lizzano, G., Casso, P., Lacave, O., Bosch, A., Bauwens, I., Knight, O.J., Potter van Loon, A., Fox, R., Parvanyan, T., Krohn Hansen, S.B., Heathfield, D., Onninen, M., Drummond, R., 2023. The global wind atlas: a high-resolution dataset of climatologies and associated web-based application. *Bull. Am. Meteorol. Soc.* 104, E1507–E1525. <https://doi.org/10.1175/BAMS-D-21-0075.1>.
- European Commission, 2020. 2050 long-term strategy - european commission [WWW Document]. URL: [https://climate.ec.europa.eu/eu-action/climate-strategies-targets/2050-long-term-strategy\\_en](https://climate.ec.europa.eu/eu-action/climate-strategies-targets/2050-long-term-strategy_en), 10.31.24.
- European Commission, 2022. REPowerEU [WWW Document]. URL: [https://ec.europa.eu/commission/presscorner/detail/en/ip\\_22\\_3131](https://ec.europa.eu/commission/presscorner/detail/en/ip_22_3131), 11.5.24.
- European Commission, 2023a. Red III, C/2023/1087 [WWW Document]. URL: <https://eur-lex.europa.eu/legal-content/EN/TXT/?uri=CELEX%3A32023R1184>.
- European Commission, 2023b. Commission delegated regulation (EU) 2023/1184 [WWW Document]. URL: <https://eur-lex.europa.eu/legal-content/EN/TXT/?uri=CELEX%3A32023R1184>.
- European Commission, 2024. Communication from the commission [WWW Document]. URL: [https://energy.ec.europa.eu/document/download/0c574279-b71d-4aa0-9403-daf9ea5a8491\\_en?filename=C\\_2024\\_5042\\_1\\_EN\\_ACT\\_part1\\_v8.pdf](https://energy.ec.europa.eu/document/download/0c574279-b71d-4aa0-9403-daf9ea5a8491_en?filename=C_2024_5042_1_EN_ACT_part1_v8.pdf).
- European Hydrogen Observatory, 2025. EU Hydrogen Strategy Under the EU Green Deal. European Hydrogen Observatory [WWW Document]. URL: <https://observatory.cle-an-hydrogen.europa.eu/eu-policy/eu-hydrogen-strategy-under-eu-green-deal>, 1.12.26.
- European Parliament, 2023. Directive (EU) 2023/2413 [WWW Document]. URL: <https://eur-lex.europa.eu/legal-content/EN/TXT/?uri=CELEX%3A32023L2413>.
- Eurostat, 2024. Statistics | Eurostat. Electricity prices for non-household consumers [WWW Document]. URL: [https://ec.europa.eu/eurostat/databrowser/view/nrg\\_pc\\_205/default/table?lang=en](https://ec.europa.eu/eurostat/databrowser/view/nrg_pc_205/default/table?lang=en), 7.16.24.
- Fasihi, M., Weiss, R., Savolainen, J., Breyer, C., 2021. Global potential of green ammonia based on hybrid PV-wind power plants. *Appl. Energy* 294, 116170. <https://doi.org/10.1016/j.apenergy.2020.116170>.
- Florez, J., AlAbbad, M., Vazquez-Sanchez, H., Morales, M.G., Sarathy, S.M., 2024. Optimizing islanded green ammonia and hydrogen production and export from Saudi Arabia. *Int. J. Hydrogen Energy* 56, 959–972. <https://doi.org/10.1016/j.ijhydene.2023.12.075>.
- Fúnez Guerra, C., Reyes-Bozo, L., Vyhmeister, E., Jaén Caparrós, M., Salazar, J.L., Clemente-Jul, C., 2020. Technical-economic analysis for a green ammonia production plant in Chile and its subsequent transport to Japan. *Renew. Energy* 157, 404–414. <https://doi.org/10.1016/j.renene.2020.05.041>.
- Gabrielli, P., Rosa, L., Gazzani, M., Meys, R., Bardow, A., Mazzotti, M., Sansavini, G., 2023. Net-zero emissions chemical industry in a world of limited resources. *One Earth* 6, 682–704. <https://doi.org/10.1016/j.oneear.2023.05.006>.
- Gomez, J.R., Baca, J., Garzon, F., 2020. Techno-economic analysis and life cycle assessment for electrochemical ammonia production using proton conducting membrane. *Int. J. Hydrogen Energy* 45, 721–737. <https://doi.org/10.1016/j.ijhydene.2019.10.174>.
- Greenhouse Gas Protocol, World Resources Institute, 2025. An amendment to the GHG protocol corporate standard GHG protocol scope 2 guidance [WWW Document]. URL: <https://ghgprotocol.org/scope-2-guidance>, 5.6.25.
- Gurobi Optimization, 2025. The Leader in Decision Intelligence Technology - Gurobi Optimization [WWW Document]. URL: <https://www.gurobi.com/>, 12.2.24.
- Hanasaki, M., Uryu, C., Daio, T., Kawabata, T., Tachikawa, Y., Lyth, S.M., Shiratori, Y., Taniguchi, S., Sasaki, K., 2014. SOFC durability against standby and shutdown cycling. *J. Electrochem. Soc.* 161, F850. <https://doi.org/10.1149/2.0421409jes>.
- Hauch, A., Ploner, A., Pylpko, S., Mougín, J., Cubizolles, G., 2020. Test and characterization of reversible solid oxide cells and stacks for innovative renewable energy storage. In: <https://doi.org/10.1002/fuce.202100046>.
- Herbinet, O., Bartocci, P., Grinberg Dana, A., 2022. On the use of ammonia as a fuel – a perspective. *Fuel Commun* 11, 100064. <https://doi.org/10.1016/J.FUECO.2022.100064>.
- IEA, 2021. Ammonia technology roadmap towards more sustainable nitrogen fertiliser production. <https://www.iea.org/reports/ammonia-technology-roadmap>.
- IEA, 2023. Indicative production costs for ammonia via electrolysis in selected regions compared to current references [WWW Document]. URL: <https://www.iea.org/g/data-and-statistics/charts/indicative-production-costs-for-ammonia-via-electrolysis-in-selected-regions-compared-to-current-references>, 12.9.24.
- Ikaheimo, J., Kiviluoma, J., Weiss, R., Holtinen, H., 2018. Power-to-ammonia in future north european 100 % renewable power and heat system. *Int. J. Hydrogen Energy*. <https://doi.org/10.1016/j.ijhydene.2018.06.121>.
- International Fertilizer Industry Association, 2024. Global ammonia production by region [WWW Document]. URL: <https://www.statista.com/statistics/1288979/global-ammonia-production-by-region/>, 10.31.24.
- IRENA, 2024. Renewable Power Generation Costs in 2023. Abu Dhabi. [https://www.irena.org/-/media/Files/IRENA/Agency/Publication/2024/Sep/IRENA\\_Renewable\\_power\\_generation\\_costs\\_in\\_2023.pdf](https://www.irena.org/-/media/Files/IRENA/Agency/Publication/2024/Sep/IRENA_Renewable_power_generation_costs_in_2023.pdf).
- IRENA, AEA, 2022. Innovation Outlook - Renewable Ammonia. Abu Dhabi, Brooklyn. <https://www.irena.org/publications/2022/May/Innovation-Outlook-Renewable-Ammonia>.
- Kakavand, A., Sayadi, S., Tsatsaronis, G., Behbahaninia, A., 2023. Techno-economic assessment of green hydrogen and ammonia production from wind and solar energy in Iran. *Int. J. Hydrogen Energy* 48, 14170–14191. <https://doi.org/10.1016/J.IJHYDENE.2022.12.285>.
- Liu, L., Fu, S., 2025. Study on decarbonizing ocean shipping propulsion power by liquid ammonia with centralized jet-flame controlled combustion strategy. *J. Clean. Prod.* 486, 144462. <https://doi.org/10.1016/J.JCLEPRO.2024.144462>.
- Luo, Y., Shi, Y., Li, W., Cai, N., 2014. Comprehensive modeling of tubular solid oxide electrolysis cell for co-electrolysis of steam and carbon dioxide. *Energy* 70, 420–434. <https://doi.org/10.1016/J.ENERGY.2014.04.019>.
- Magnino, A., Marocco, P., Santarelli, M., Gandiglio, M., 2025. Economic viability and CO2 emissions of hydrogen production for ammonia synthesis: a comparative analysis across Europe. *Adv. Appl. Energy* 17, 100204. <https://doi.org/10.1016/J.ADAPEN.2024.100204>.
- Maps, Electricity, 2024. Electricity Maps | Emissioni Di CO2 in Tempo Reale Del Consumo Elettrico [WWW Document]. URL: <https://app.electricitymaps.com/map?lang=it>, 7.12.24.
- Marocco, P., Ferrero, D., Martelli, E., Santarelli, M., Lanzini, A., 2021. An MILP approach for the optimal design of renewable battery-hydrogen energy systems for off-grid

- insular communities. *Energy Convers. Manag.* 245, 114564. <https://doi.org/10.1016/j.enconman.2021.114564>.
- Marocco, P., Gandiglio, M., Santarelli, M., 2026. Optimising green hydrogen production across Europe: how renewable energy sources shape plant design and costs. *Renew. Energy* 256, 124542. <https://doi.org/10.1016/J.RENENE.2025.124542>.
- Mayer, P., Ramirez, A., Pezzella, G., Winter, B., Sarathy, S.M., Gascon, J., Bardow, A., 2023. Blue and green ammonia production: a techno-economic and life cycle assessment perspective. *iScience* 26. <https://doi.org/10.1016/J.ISCI.2023.107389/ATTACHMENT/4363DE6C-D06E-405B-8513-CC8B2B2F70FC/MMC1.PDF>.
- McKinsey, 2023. Reducing GHG emissions with green ammonia and fertilizer [WWW Document]. URL. [https://www.mckinsey.com/industries/agriculture/our-insights/from-green-ammonia-to-lower-carbon-foods#/, 7.31.24](https://www.mckinsey.com/industries/agriculture/our-insights/from-green-ammonia-to-lower-carbon-foods#/).
- Mingolla, S., Gabrielli, P., Manzotti, A., Robson, M.J., Rouwenhorst, K., Ciucci, F., Sansavini, G., Klemun, M.M., Lu, Z., 2024. Effects of emissions caps on the costs and feasibility of low-carbon hydrogen in the European ammonia industry. *Nat. Commun.* 15, 1–23. <https://doi.org/10.1038/s41467-024-48145-z>, 2024.
- Morgan, E.R., Manwell, J.F., McGowan, J.G., 2017. Sustainable ammonia production from U.S. offshore wind farms: a techno-economic review. *ACS Sustain. Chem. Eng.* 5, 9554–9567. <https://doi.org/10.1021/acssuschemeng.7b02070>.
- Mukelabai, M.D., Gillard, J.M., Patchigolla, K., 2021. A novel integration of a green power-to-ammonia to power system: reversible solid oxide fuel cell for hydrogen and power production coupled with an ammonia synthesis unit. *Int. J. Hydrogen Energy* 46, 18546–18556. <https://doi.org/10.1016/J.IJHYDENE.2021.02.218>.
- Nami, H., Rizvandi, O.B., Chatzichristodoulou, C., Hendriksen, P.V., Frandsen, H.L., 2022. Techno-economic analysis of current and emerging electrolysis technologies for green hydrogen production. *Energy Convers. Manag.* 269, 116162. <https://doi.org/10.1016/J.ENCONMAN.2022.116162>.
- Nayak-Luke, R.M., Bañares-Alcántara, R., 2020. Techno-economic viability of islanded green ammonia as a carbon-free energy vector and as a substitute for conventional production. *Energy Environ. Sci.* 13, 2957–2966. <https://doi.org/10.1039/D0EE01707H>.
- Nayak-Luke, R., Bañares-Alcántara, R., Wilkinson, I., 2018. “green” ammonia: impact of renewable energy intermittency on plant sizing and leveled cost of ammonia. *Ind. Eng. Chem. Res.* 57, 14607–14616. [https://doi.org/10.1021/ACS.IECR.8B02447/ASSET/IMAGES/LARGE/IE-2018-02447Z\\_0007.JPEG](https://doi.org/10.1021/ACS.IECR.8B02447/ASSET/IMAGES/LARGE/IE-2018-02447Z_0007.JPEG).
- Nejadian, M.M., Ahmadi, P., Houshfar, E., 2022. Comparative optimization study of three novel integrated hydrogen production systems with SOEC, PEM, and alkaline electrolyzer. *Fuel*. <https://doi.org/10.1016/j.fuel.2022.126835>.
- Nowicki, D.A., Agnew, G.D., Irvine, J.T.S., 2023. Green ammonia production via the integration of a solid oxide electrolyzer and a haber-bosch loop with a series of solid electrolyte oxygen pumps. *Energy Convers. Manag.* 280, 116816. <https://doi.org/10.1016/J.ENCONMAN.2023.116816>.
- Salmon, N., Bañares-Alcántara, R., 2021. Impact of grid connectivity on cost and location of green ammonia production: australia as a case study. *Energy Environ. Sci.* 14, 6655–6671. <https://doi.org/10.1039/D1EE02582A>.
- Schiedeck, M., Nogueira Nakashima, R., Frandsen, H.L., 2025. Heat integration and part-load performance of an SOEC-coupled haber–bosch process. *Int. J. Hydrogen Energy* 116, 242–256. <https://doi.org/10.1016/J.IJHYDENE.2025.02.335>.
- Schwarze, K., Geißler, T., Nimtz, M., Blumentritt, R., 2023. Demonstration and scale-up of high-temperature electrolysis systems. *Fuel Cells* 23, 492–500. <https://doi.org/10.1002/FUCE.202300059>.
- SFI, 2023. Petrochemicals - UK centre for greening finance and investment (CGFI) [WWW Document]. URL. <https://www.cgfi.ac.uk/spatial-finance-initiative/geoasset-project/petrochemicals/>, 4.16.25.
- Solargis, World Bank Group, 2025. Energy Sector Management Assistance Program. Global Solar Atlas [WWW Document]. URL. <https://globalsolaratlas.info/map>, 1.14.26.
- Soloveichik, G., 2019. Electrochemical synthesis of ammonia as a potential alternative to the haber–bosch process. *Nat. Catal.* 25 (2), 377–380. <https://doi.org/10.1038/s41929-019-0280-0>, 2019.
- Sousa, J., Waiblinger, W., Friedrich, K.A., 2022. Techno-economic study of an electrolysis-based green ammonia production plant. *Ind. Eng. Chem. Res.* 61, 14515–14530. <https://doi.org/10.1021/ACS.IECR.2C00383>.
- Sunfire, 2024. The electrolysis specialist Sunfire-HyLink SOEC [WWW Document]. URL. [https://sunfire-backend.pechschwarz.dev/wp-content/uploads/2024/10/Sunfire\\_Fact-Sheet\\_SOEC\\_EN\\_digital.pdf](https://sunfire-backend.pechschwarz.dev/wp-content/uploads/2024/10/Sunfire_Fact-Sheet_SOEC_EN_digital.pdf), 10.24.24.
- Sunfire, 2025. World's largest SOEC electrolyzer startet up at neste's rotterdam refinery [WWW Document]. URL. <https://sunfire.de/en/news/worlds-largest-soec-electrolyzer-startet-up-at-nestes-rotterdam-refinery/>, 1.7.26.
- Suryanto, B.H.R., Matuszek, K., Choi, J., Hodgetts, R.Y., Du, H.L., Bakker, J.M., Kang, C.S.M., Cherepanov, P.V., Simonov, A.N., MacFarlane, D.R., 2021. Nitrogen reduction to ammonia at high efficiency and rates based on a phosphonium proton shuttle. *Science* 372, 1187–1191. <https://doi.org/10.1126/SCIENCE.ABG2371>.
- Wang, C., Walsh, S.D.C., Longden, T., Palmer, G., Litalo, I., Dargaville, R., 2023. Optimising renewable generation configurations of off-grid green ammonia production systems considering haber–bosch flexibility. *Energy Convers. Manag.* 280, 116790. <https://doi.org/10.1016/j.enconman.2023.116790>.
- Wang, H., Zhou, P., Jeong, B., Mesbahi, A., Mujeeb-Ahmed, M.P., Jang, H., Giannakis, A., Sykaras, K., Papadakis, A., 2025. Life cycle analysis of ammonia fuelled ship – case ship studies for marine vessels. *J. Clean. Prod.* 520, 146105. <https://doi.org/10.1016/J.JCLEPRO.2025.146105>.
- Wolf, S.E., Winterhalder, F.E., Vibhu, V., de Haart, L.G.J., Guillon, O., Eichel, R.A., Menzler, N.H., 2023. Solid oxide electrolysis cells - current material development and industrial application. *J. Mater. Chem. A* 11, 17977–18028. <https://doi.org/10.1039/d3ta02161k>.
- Wu, Z.Y., Karamad, M., Yong, X., Huang, Q., Cullen, D.A., Zhu, P., Xia, C., Xiao, Q., Shakouri, M., Chen, F.Y., Kim, J.Y. (Timothy), Xia, Y., Heck, K., Hu, Y., Wong, M.S., Li, Q., Gates, I., Siahrostami, S., Wang, H., 2021. Electrochemical ammonia synthesis via nitrate reduction on Fe single atom catalyst. *Nat. Commun.* 12, 1–10. <https://doi.org/10.1038/s41467-021-23115-x>, 2021.
- Yoshida, M., Ogawa, T., Imamura, Y., Ishihara, K.N., 2021. Economies of scale in ammonia synthesis loops embedded with iron- and ruthenium-based catalysts. *Int. J. Hydrogen Energy* 46, 28840–28854. <https://doi.org/10.1016/j.ijhydene.2020.12.081>.
- Yu, Z., Lin, J., Liu, F., Li, J., Zhao, Y., Song, Y., 2024. Optimal sizing of isolated renewable power systems with ammonia synthesis: model and solution approach. *IEEE Trans. Power Syst.* 39, 6372–6385. <https://doi.org/10.1109/TPWRS.2024.3360315>.
- Zhang, H., Wang, L., Van herle, J., Maréchal, F., Desideri, U., 2020. Techno-economic comparison of green ammonia production processes. *Appl. Energy* 259, 114135. <https://doi.org/10.1016/J.APENERGY.2019.114135>.
- Zumdahl, S.S., 2024. Ammonia | Definition & Uses | Britannica. *Encycl. Br.* <https://www.britannica.com/science/ammonia>.